Journal of Hydrology 622 (2023) 129744

Contents lists available at ScienceDirect

Journal of Hydrology

journal homepage: www.elsevier.com/locate/jhydrol

Research papers

Field-based monitoring of instream leaky barrier backwater and storage during storm events

Valentine Muhawenimana [a,*], Elizabeth Follett [a], Ian Maddock [b], Catherine A.M.E. Wilson [a]

[a] Cardiff School of Engineering, Cardiff University, Cardiff CF24 3AA, UK
[b] School of Science and the Environment, University of Worcester, Worcester WR2 6AJ, UK

ARTICLE INFO

Keywords:
Natural flood management
Leaky barrier
Flood attenuation
Backwater rise, Barrier storage

ABSTRACT

Engineered leaky barriers are increasingly used as natural flood management methods providing ecosystem and water quality benefits in addition to flood attenuation, complementing hard engineering flood defences. Field-based monitoring of a natural flood management site, Wilde Brook in the Corvedale catchment, England (UK) studied the rainfall-runoff relationship for a 5.36 km reach with 105 leaky barriers over two years. Paired pressure transducers were placed upstream and downstream of three channel spanning leaky barriers, allowing evaluation of upstream backwater rise relative to rainfall intensity, storm magnitude, and frequency. By increasing backwater rise, the leaky barriers caused overbank flows, resulting in a reduction in the cross-sectional area velocity after the event. The incidence of overbank flow depended on the local stream cross-sectional profile, barrier properties, location in the reach, and storm magnitude. Barrier operational flow conditions were classified into five modes according to relative bank inundation and barrier submergence extent. The backwater rise magnitude depended on barrier physical properties and evolution over time through cycles of accretion and build-up of brash and leafy material in the barrier, in addition to local bedload sediment transport dynamics, where instances of scour around the barriers were observed. Backwater rise and net volume hydrographs showed rapid filling up behind the barriers on the rising limb and slower water release on the falling limb. For a ~ 4 yr return period storm event, results indicated that one leaky barrier increased storage volume by up to 102 m^3, which translates to an overall net volume increase of ~ 10,700 m^3 for the full reach. These new findings provide quantitative evidence of leaky barrier backwater and storage performance, and leaky barrier design recommendations for storms up to a 4 yr return period. This evidence can be used to develop and validate flood modelling generalised approaches for smaller, more frequent storms, and work towards the development of an approach for modelling leaky barriers for larger storm magnitudes.

1. Introduction

Flood disasters remain a challenging global problem, with extreme human and socio-economic costs, and flood risk further worsened by expected increases in storm intensity and flooding due to climate change (IPCC 2014). Flood defences traditionally use hard engineering methods to mitigate flood risk. In order to add flood resilience, nature-based solutions to flooding or Natural Flood Management (NFM) utilises natural catchment process methods in upper catchments to reduce and delay low return period flood peaks further downstream (Burgess-Gamble et al., 2017, Dadson et al. 2017). NFM interventions additionally benefit surface and groundwater quality by reconnecting fragmented watercourses, increasing wet spaces, and creating more heterogenous spaces for wildlife, therefore enhancing biodiversity (Faustini and Jones, 2003; Bouwes et al., 2016; Wohl et al., 2016).

These soft engineering methods include runoff attenuation instream structures such as wood leaky barriers, which slow down, temporally store and gradually release flood flows, therefore reducing downstream flood levels and attenuating flood peaks (Burgess-Gamble et al., 2017). Studies evaluating leaky barrier performance quantify effectiveness using the following metrics: reduction in downstream peak flow, reduction in downstream water level, delay in downstream peak flow and increase in catchment response time (Burgess-Gamble et al., 2017, Keys et al., 2018, Black et al., 2020). Field monitoring case studies have reported that leaky barriers achieve 27% peak outflow discharge reduction (Norbury et al., 2021). A time lag of ten minutes on the

* Corresponding author.
E-mail address: MuhawenimanaV@cardiff.ac.uk (V. Muhawenimana).

https://doi.org/10.1016/j.jhydrol.2023.129744
Received 17 February 2023; Received in revised form 21 May 2023; Accepted 24 May 2023
Available online 31 May 2023

outflow peak discharge for a 3.5 year return period storm event, was estimated for a one kilometre reach based on upscaling results from a small experimental test channel with a single wood barrier (Wenzel et al, 2014). While an increase in the delay of times of peak discharge compared to observed rainfall peaks ranging from 2.6 to 7.3 h have been observed at a catchment scale for a mixture of leaky barriers, storage ponds and woodland planting (Black et al., 2020). Modelling studies also estimate peak outflow discharge reduction for reaches ranging from 4% (Hankin et al., 2019) to 11% (Metcalfe et al., 2017), and 30% (Nicholson et al., 2020) at a catchment scale for leaky barriers used in conjunction with other NFM measures.

The role of large wood in increasing heterogeneity of flow and regulating sediment transport in the river landscape has been recognised with the reintroduction of wood and wood retention in river restoration and river management practices (Nisbet et al., 2011; Bouwes et al., 2016; Burgess-Gamble et al., 2017; Dadson et al., 2017; Black et al., 2020; Norbury et al., 2021). In such practices the benefits of ecological improvement are balanced with impacts on channel conveyance and flood management. Previous studies have given insight into the dynamic interrelationships between flow hydraulics, and wood patch morphology and channel morphology.

The structure of wood barriers has been observed to change over time through the accumulation and depletion of organic material, and local scour and deposition of bedload sediment, which alters the surrounding channel and bank morphology (Gibling et al., 2010; Wohl and Beckman, 2014; Dixon and Sear, 2014; Wohl and Iskin, 2022). Changes to the wood barrier and channel morphology result in changes in backwater rise over time (Geertsema et al., 2020) and supports previous studies that observed backwater rise magnitude to be a function of the wood patch height (Curran and Wohl 2003; Wilcox and Wohl 2006). The backwater rise-discharge relationship for large wood barriers on a streambed has been characterised by a steeper increase in backwater rise with increasing discharge until a threshold is reached related to the barrier geometry and channel profile, after which the increase in backwater rise declines (Geertsema et al, 2020). The backwater rise has been related to the barrier physical structure with momentum loss proportional to the number, size, and packing density of the logs and the barrier length, and lower gap width, allowing description of barriers with a common structural metric and development of a rating curve for depths below the barrier crest (Follett et al., 2020, Follett et al., 2021). However, research gaps remain for the effect of barriers at water depths above the barrier crest and the impact of barriers during periods of unsteady flow. In this paper the impact of barriers for water depths above the barrier crest and unsteady flow conditions is examined using monitoring evidence from a natural flood management site.

Wood barriers generate an increase in flood peak lag time by increasing upstream water depth and local floodplain water storage (Burgess-Gamble et al., 2017; Keys et al., 2018; Follett et al., 2020, Follett et al., 2021; Muhawenimana et al., 2021) Wood barriers also alter the transport of bedload and channel bank sediment (Schalko et al., 2019; Follett and Wilson, 2020), and increase hydraulic roughness (Wilcox and Wohl 2006; Geertsema et al., 2020, Follett and Hankin 2022). Evaluation of the effectiveness of leaky barriers is still advancing, with few studies attempting to quantify the functional behaviour of leaky barriers, water storage potential and how their evolution impacts on their function (Wenzel et al, 2014, Burgess-Gamble et al., 2017). In addition, empirical evidence is still lacking to quantify the hydraulic impact of leaky barriers at the structure and reach scales. There is little practical guidance on leaky barrier design and its optimisation for flood risk management purposes. This information is crucial for stakeholders for NFM scheme design and facilitating the wider use of NFM in flood risk management.

In this paper we present new field monitoring evidence of a natural flood management site comprising 105 leaky barriers on the Wilde Brook, Corvedale, Shropshire, UK. This scheme is one of the 26 fluvial natural flood management 'monitoring' projects funded by the UK Government in 2018 with the key aim of "learning by doing" (Arnott et al., 2018). Using a flow sensor, rain gauge, and paired water level loggers upstream and downstream of the leaky barriers in three locations along the reach, we evaluate the hydraulic effect of the leaky barriers for storm events recorded over a two-year monitoring duration, relative to the local channel bathymetry. The rise in upstream backwater and water storage volume are compared between barriers with different physical characteristics for selected storm events. The new evidence on leaky barrier operation will inform the planning and design stages of future flood risk management projects.

2. Methods

2.1. Field site description

The Wilde Brook monitored test reach site is 5.36 km in length and has a catchment area of 5.3 km^2. It is bounded on the north-west by Wenlock Edge, which is limestone escarpment and a site of special scientific interest due to its geology (England, 1986). The catchment's land use is comprised of agricultural land with a mix of pasture and arable. Wilde Brook is one of eight tributaries of the River Corve in the Coverdale catchment in Shropshire, England (Fig. 1).

The upstream section of the Wilde Brook reach is referred to as the Wilderhope Upper reach, while the Wilderhope Middle reach refers to the section of the reach prior to the confluence with an ephemeral stream at the Upper confluence (Fig. 1). The Wilderhope Lower reach indicates the section of the reach between the Upper confluence and the downstream Corve Confluence (Fig. 1). Sequentially, the streamwise distances of reach segments between measurement locations from the upstream end of Wilde Brook to Wilderhope Upper is 870 m, from Wilderhope Upper to Wilderhope Middle is 758 m, 888 m from Wilderhope Middle to Upper Confluence, 1,426 m from Upper Confluence to Wilderhope Lower 2, 26 m from Wilderhope Lower 2 to Wilderhope Lower 1, 784 m from Wilderhope Lower 1 to Flow site velocity sensor, which is 617 m to Corve Confluence.

2.2. Monitoring instrumentation: Paired pressure transducers, rain gauge, and flow meter

Hydrometric monitoring instrumentation was first installed in April-May 2019 and georeferenced using DGPS and regularly checked

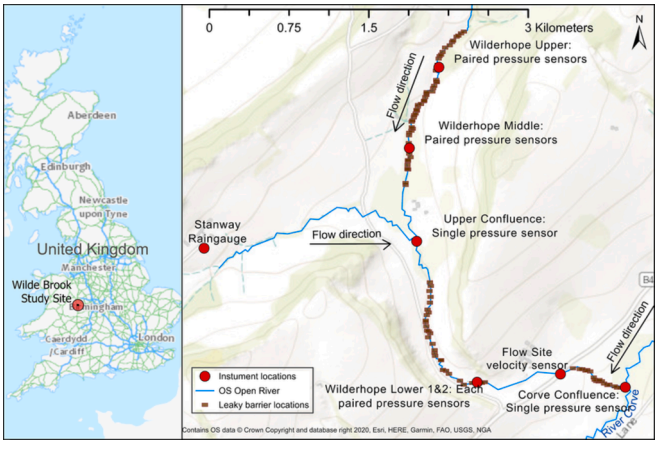

Fig. 1. Wilde Brook site map showing locations of 105 leaky barriers (solid dark brown squares). Location of Wilderhope Upper, Wilderhope Middle, and Wilderhope Lower 1 & 2 paired pressure sensors, Upper Confluence and Corve Confluence single pressure sensors, Flow Site velocity sensor, and Stanway Raingauge indicated by solid red circles. Flow direction indicated by black arrow. (For interpretation of the references to colour in this figure legend, the reader is referred to the web version of this article.)

manually and maintained. The monitoring instrumentation consisted of 10 vented pressure transducers (OTT Orpheus Mini pressure level sensor) of which eight were paired, located 2.4–4 m upstream and downstream of the selected leaky barriers in the Wilderhope Upper, Wilderhope Middle, and Wilderhope Lower reaches and two were placed as single pressure sensors at the Wilderhope Upper Confluence and Corve Confluence (Fig. 1). The pressure transducers recorded water levels every 15 min, with an accuracy of ± 0.05 % (OTT, 2021). Rainfall was recorded at the Stanway Raingauge station (Fig. 1) using a Lambrecht Tipping Bucket raingauge, which recorded 0.2 mm events at 15 min intervals. Due to low battery voltage, there is a gap in the data from 11 April 2020 and 29 May 2020. The data and analysis presented in this paper relates to the period 12 April 2019 to 22 June 2021.

The investigation of the barrier at Wilderhope Lower 2 did not commence until November 2020 when the paired pressure transducers were installed. Therefore Lower 2 is not included in the current analysis to ensure consistency in the monitoring durations for the paired leaky barriers. Hereafter, Wilderhope Lower refers to the Wilderhope Lower 1 barrier.

A flow meter (AV 9000 Area Velocity Sensor with a Hach FL900 Flow Logger) was placed downstream of a culvert (1.57 m wide and 1.1 m high), indicated as Flow Site velocity sensor in Fig. 1. The flow logger recorded water level, flow velocity and discharge at 15 min intervals. Battery malfunctions occurred for the flow logger, and battery replacement did not resolve data quality issues. Therefore, only flow data from April-September 2019 is presented here. The recorded discharge data was fitted to the rating curve equation $Q = 1.6525H^{2.6102}$ $R^2 = 0.99$, where Q is discharge (m^3/s) and H is water depth (m). The uncertainty in estimated discharge associated with using a rating curve derived from a short record length is acknowledged, and the discharge uncertainty was determined. The ReFH approach (version 2) was used to estimate the flood frequency of each peak river discharge (Kjeldsen, 2007; Wallingford HydroSolutions, 2021). The return period estimates provided an indicative magnitude for the observed storm events, placing them within a flood frequency context. Four substantial storm events observed during the two-year monitoring period are highlighted in this paper: ~2 yr return period events on 19 December 2019 and 14 November 2019, and 4 yr return period events on 26 October 2019 and 16 February 2020.

2.3. Leaky barrier properties and local channel bathymetry

105 leaky barriers were constructed on the Wilde Brook monitored test reach between Winter 2016 and February 2018, using wood (Alder, Hazel and Oak species) sourced locally from the riverbanks and floodplain. The longitudinal spacing between barriers varied from 11 to 50 m, while the vertical gap below the barriers varied between zero to 0.75 m. The leaky barriers consisted of channel spanning key members as well as secondary members of varying diameters and lengths. The channel-spanning members were secured using wooden pegs and rebar, and anchored to bankside tree trunks where available. A vertical gap above the bed was maintained below the barriers to ensure free passage of baseflow. The majority of designs followed available engineered barrier guidance (ADEPT, 2019), which were adapted for specific channel cross-sections (Neal L., personal communication, 14 September 2021). The most frequent leaky barrier design consisted of channel spanning parallel large logs placed perpendicular to the main flow direction and pinned in place, while other barriers consisted of smaller logs and tree branches resembling natural woody accumulations where the logs were accumulated rather than engineered in geometrical arrangement, and others were built as woven structures. The barriers were georeferenced and their characteristics including elevation above bed, number of key members, composition and size were measured. Photographic records of the barriers were collected annually to track their time evolution. Natural accretion and washout or depletion of brash material from the leaky barriers was allowed to take place. Maintenance of the leaky barriers was carried out only when key members became dislodged or moved, usually during higher flow events, which occurred for 10% of the leaky barriers since installation. Leaky barrier repairs were carried out in Winter 2020 (Neal L., personal communication, 10 December 2021).

2.4. Description of the selected leaky barriers with paired pressure transducers

Three sets of paired pressure transducers measured the sensor submergence depth upstream and downstream of three leaky barriers located in the Wilderhope Upper, Wilderhope Middle and Wilderhope Lower sub reaches, beginning on 12 April 2019. These three paired leaky barriers were selected to represent a range of leaky barrier designs, barrier-bank profiles, and bed slopes at various stations along the reach. The water surface elevation was measured relative to a yellow survey peg georeferenced at installation and during four service visits (November 2019, May 2020, November 2020, July 2021, September 2021). Barrier vertical extent, visually apparent structural composition, accumulation of brash and leaves, and visually apparent bedload sediment transport were observed at field visits (February 2019, November 2019, November 2020, July 2021, September 2021) through repeat photographs of the barriers and survey measurements using a wading rod to an accuracy of ±1 cm. Stream cross-section profiles were surveyed in November 2020 at the location of the pressure transducers. The channel right-hand side (RHS) and left-hand side (LHS) are defined looking in the downstream flow direction.

Characteristics of the Wilderhope Upper, Middle and Lower barriers are shown in Table 1, and photographs of the barriers are shown in Fig. 2. The Wilderhope Upper measurement site comprised of a barrier composed of two logs placed across the upper channel and pinned upstream and downstream on both banks with wooden stakes. No changes in bed level due to bedload sediment transport were visually apparent during the monitoring period. The Wilderhope Middle measurement site leaky barrier comprised a woven structure perpendicular to the flow direction. At the Wilderhope Lower measurement site, the barrier used a naturalised engineered design composed of a varied accumulation of logs constructed perpendicular to the flow direction. Table 2 shows the channel cross-sections at the pressure loggers upstream of each barrier.

2.5. Wilde brook structure-from-motion (SfM) photogrammetry

To obtain ultra-high spatial resolution topographic survey data of a sub-reach of the Wilderhope Lower site (Fig. 1) that has significant canopy cover, pole-mounted photography (Gonçalves et al., 2016, Luhmann et al., 2019) supplemented with imagery from an Uncrewed Aerial System (UAS) where feasible was utilised. Structure-from-Motion (SfM) photogrammetry was applied to a sub-reach 130 m long (reach length defined as measured along the thalweg) that included five leaky barriers. The field survey was conducted at low flow in March 2021 which enabled an uninhibited view of the stream bed through the clear and shallow water. Initially, 26 ground control points were placed along the channel margins and their locations surveyed with the Trimble R10 RTK GPS. Pole-mounted images were obtained with a DJI Phantom 4 RTK UAS attached with clamps to two extendable carbon fibre poles, with image locations corrected with connection to a DJI D-RTK 2 GNSS base station located within 50 m of the surveyed reach. Images were taken at a height of ~ 3 m above the ground at an oblique angle of 75° spaced approximately every 0.4 m along each bank in order to create ~ 80% overlap between images. Additional nadir imagery was collected by carefully flying the UAS under the canopy and above the water surface at a height of approximately 3 m above the channel wherever possible. SfM photogrammetry was applied to the resulting 825 images using Agisoft Metashape 1.7.3 to create a dense point cloud (consisting of 389,815,240 points), Digital Elevation Model (DEM) and orthophotomosaic. Refraction correction was applied to the submerged areas in

Table 1
Leaky barrier characteristics including the number of main logs and their range of diameters, the gap beneath the barrier and the height above the bed, and streamwise length in the direction of flow (L_s) of the barrier. LHS and RHS indicate the left-hand side and right-hand side of the barrier, respectively. Photographs of barrier designs for Wilderhope Upper, Middle and Lower are shown in Fig. 2.

	Logs comprising barrier				Barrier height (m)		
	Number	diameters (m)	Bottom gap (m)	Ls (m)	LHS	Centre	RHS
Wilderhope Upper	2	0.2, 0.4	0.48–0.5	1.1[a]	0.9	0.85	0.7
Wilderhope Middle	11	0.045–0.05[c] 0.05–0.12[d]	0.05	0.7[a]		0.96	
Wilderhope Lower	3	0.45, 0.15, 0.03	0.1	1.2–2.3[b]		1.1	

[a] July 2021, [b]September 2021 streamwise barrier length (L_s) measurements, [c]vertical main logs, [d]horizontal main logs.

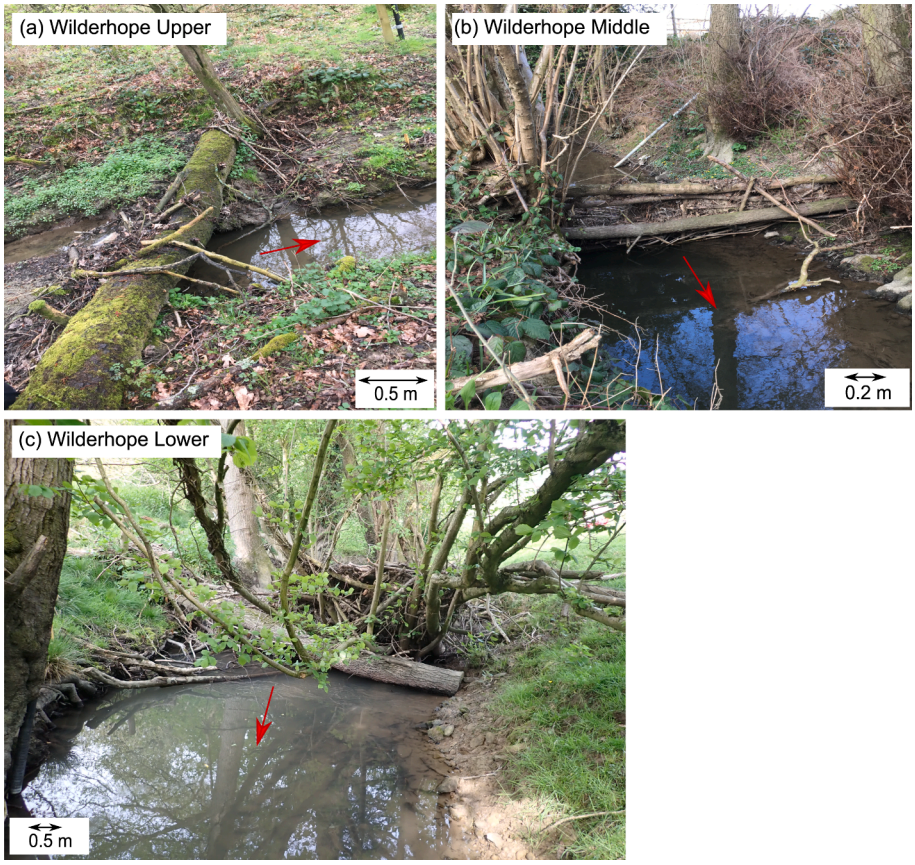

Fig. 2. Photographs of leaky barriers (a) Wilderhope Upper, (b) Wilderhope Middle in February 2021 and (c) Wilderhope Lower in May 2022. Main channel widths at the location of the barriers were 1.61, 5.1, and 2.6 m for the Upper, Middle and Lower barriers, respectively. The red arrows indicate the flow direction. (For interpretation of the references to colour in this figure legend, the reader is referred to the web version of this article.)

Table 2
Channel cross-section widths for main channel (bankfull) and floodplains at the location of the pressure logger upstream and downstream of Wilderhope Upper, Middle and Lower barriers. Upstream and downstream bankfull depths are given for the main channel banks and refer here to the lowest bank in the channel section.

	Upstream channel section				Downstream channel section			
	Channel width (m)			Bankfull depth (m)	Channel width (m)			Bankfull depth (m)
	Main channel	Floodplain LHS	Floodplain RHS	Main channel	Main channel	Floodplain LHS	Floodplain RHS	Main channel
Wilderhope Upper	1.7	0.7	3.4	0.47	1.64	2.8	3.5	0.50
Wilderhope Middle	5.5			1.15	5.1			1.39
Wilderhope Lower	3.1	2.6	3.7	1.07	2.6	2.3		0.984

the DEM following established procedures (Westaway et al., 2000, Woodget et al., 2015). The DEM has a spatial resolution of 2 mm/pixel, a point density of approximately 25 points per cm^2 and its positional accuracy had a root mean square error (RMSE) of 2 cm in the horizontal direction, and 4 cm vertically.

2.6. Storage volume calculation

2.6.1. Using SfM photogrammetry-derived DEM for the Wilderhope lower sub-reach

Water volumes stored upstream of the Wilderhope Lower leaky barrier for a given water level were calculated by trapezoidal numerical

integration over the meshgrid interpolated from the SfM photogrammetry-derived (2 mm resolution) DEM using MATLAB R2021a. The area of interest was delimited from the upstream face of the leaky barrier of interest, to the downstream face of the leaky barrier immediately upstream. The measured upstream pressure transducer water level was assumed to be horizontal over this area and applied to the trapezoidal interpolation of volumes. Local cross-sections from the DEM at the pressure transducer location were verified with bed survey transects. The trapezoidal integration was performed for submerged areas of the DEM only, i.e., areas with water elevation greater than bed elevation. The net storage volume represents the difference between the estimated storage volume upstream and downstream of the leaky barrier, or the increase in storage volume attributed to the leaky barrier. Similarly, the trapezoidal integration method was used to calculate the flow velocity upstream of the leaky barriers, using the stream cross-section profiles, the measured water level, the flow cross-section area, and the discharge recorded at the Flow Site velocity sensor.

2.6.2. Using 2 m DTM Lidar data

The SfM photogrammetry-derived DEM provided an ultra-high resolution survey of the majority of the modelled reach at the Wilderhope Lower monitoring location. However, for flood inundation exceeding the upstream extent of the SfM photogrammetry-derived DEM, Ordnance Survey 2 m DTM Lidar from the Environment Agency with accuracy of +/-15 cm RMSE (Lidar Composite Digital Terrain Model England 2m resolution, 2016, EDINA LiDAR Digimap Service, https://digimap.edina.ac.uk) was used to evaluate the water volume upstream of the leaky barrier of interest. The coordinates for each LiDAR tile were obtained using lower left corner × and y coordinates for the given elevation. The resulting matrix was then reshaped into column arrays, which could be used to create a meshgrid of the bathymetry. The trapezoidal interpolation method outlined in Section 2.6.1 was used to obtain the water volume stored inbank and overbank upstream of the leaky barrier using the LiDAR meshgrid. Processing and analysis were again conducted using MATLAB R2021a.

3. Results

3.1. Rainfall intensity

Hourly cumulative rainfall is shown in Fig. 3 (grey circles), where the Wilderhope Lower upstream and downstream paired pressure transducer submergence depths at the time of the rainfall record are also plotted (Fig. 3, black and blue solid lines). Several heavy rainfall events with daily rainfall magnitude greater than 20 mm per day occurred during the monitoring period, as shown in Table 3 along with storm names available from the UK's Met Office. The highest recorded daily rainfall intensity reached 41.6 mm/day on 11 June 2019, and the second and third highest intensity were 37.6 mm/day on 26 October 2019, and 35.2 mm/day on 12 August 2020, respectively. The 12 August 2020 event showed the maximum recorded hourly rainfall intensity of 22.6 mm/hour. Named storms of lesser magnitude were also recorded, including Storm Jorge (28 February −01 March 2020) and Storm Ellen (19–20 August 2020) with recorded intensity of 10.6 mm/day and 19.6 mm/day, respectively (UK storm season 2019/20 – Met Office). Key rainfall and storm events recorded are shown chronologically in Table 3, with their duration, rainfall intensity and lag time between rainfall and discharge centroids.

3.2. Paired pressure transducer water levels

Time series of sensor submergence depths recorded at paired pressure transducers upstream of three leaky barriers in the Wilderhope Upper, Wilderhope Middle and Wilderhope Lower sub reaches are shown in Fig. 4, where upstream LHS and RHS channel banks are indicated. The water levels relative to the channel banks indicated the occurrence of inbank, bankfull, partial overbank (only one bank is inundated) and fully overbank events.

A wide range of inundation levels were observed at the Wilderhope Upper site (Fig. 4a), including inbank flows below both RHS and LHS banks upstream and downstream of the barrier, partial overbank flows where the water spilled over only the RHS bank upstream of the barrier, and fully overbank events where both RHS and LHS banks were simultaneously inundated upstream of the barrier. Partial overbank events occurred on 23–24 February, 16 December 2020, and 30 January 2021. Fully overbank events occurred on 12–13 June, 25–26 October, 14–17 November, 19 December 2019, 15–16 February 2020, 23 and 27 December 2020, 20–21 and 28 January 2021, 2 February 2021 and 13 May 2021. Over the 802 days of monitoring, partial overbank events at the Upper site totalled 130 h (0.68% of total record time), while full bank inundation lasted a total of 47.75 h (0.25% of total record time). Downstream of the barrier, inundation of the RHS bank occurred on 26 October 2019, and both RHS and LHS banks were inundated during Storm Dennis on 16 February 2020.

At the Wilderhope Middle site (Fig. 4c), flows remained inbank for the majority of the monitoring time for 97.09% of the total record time, with partial overbank flows inundating the upstream RHS bank for 560 h i.e., 2.91% of the total record time. Due to the incised profile of the stream at the Middle site, the LHS bank was not inundated during the monitoring period. The downstream RHS was inundated during Storm

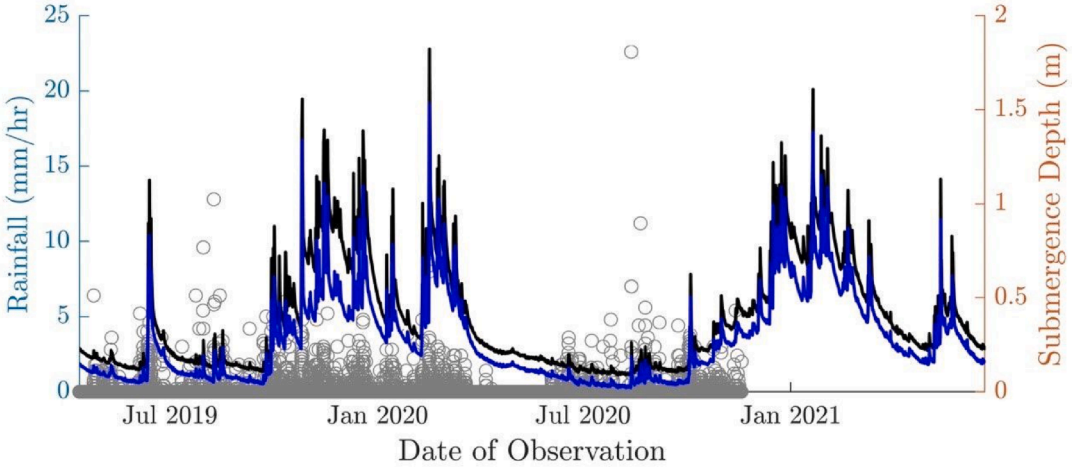

Fig. 3. Time series of daily and hourly rainfall (left y axis), upstream (black) and downstream (blue) sensor submergence depths (right y-axis) for the Wilderhope Lower 1 paired pressure transducers. (For interpretation of the references to colour in this figure legend, the reader is referred to the web version of this article.)

Table 3
Recorded high rainfall events (daily rainfall greater than 20 mm) and corresponding Met Office storm name reference. Lag time is the time difference between the centroids of discharge and rainfall for each storm event. "-" is shown for events where discharge data was unavailable.

Date Observed	Rainfall (mm/day)	Storm duration (hr)	Rainfall intensity (mm/hr)	Lag time (hr)	Storm name: Met Office
11/06/2019	41.6	92	1.02	18.22	Heavy rainfall (11–144 June 2019)
12/06/2019	27.4				Heavy rainfall (11–144 June 2019)
30/07/2019	25.8	10	2.56	9.46	Local storm
09/08/2019	23.8	37	1.15	16.26	Local storm
25/10/2019	32.8	30	2.35	4.11	Heavy rainfall (25–26 October 2019)
26/10/2019	37.6				Heavy rainfall (25–26 October 2019)
14/11/2019	33.2	34	1.13	6.74	Local storm
19/12/2019	23.6	46	0.8	1.99	Local storm
09/02/2020	20.8	50	0.59	4.05[a]	Storm Ciara (08–09 February 2020)
15/02/2020	23.6	60	0.98	6.15	Storm Dennis (144–16 February 2020)
16/02/2020	33.6				Storm Dennis (144–16 February 2020)
12/08/2020	35.2	7	5.5	–	Local storm
25/08/2020	24.6	23	1.1	–	Storm Francis (25 August 2020)
03/10/2020	27	60	1.2	–	Storm Alex (2–4 October 2020)
04/10/2020	21.6				Storm Alex (2–4 October 2020)

[a] indicates antecedent conditions.

Dennis (15–16 February 2020).

At the Wilderhope Lower site (Fig. 4e), similarly due to the steepness of the bank, the RHS downstream bank was not inundated during the monitoring period, while both the upstream and downstream LHS banks were only inundated, i.e., fully overbank during Storm Dennis (15–16 February 2020) for 2.5 h. The total time occupied by partial overbank events totalled 540.75 h i.e., 2.81% of total record time, the majority of which occurred during autumn and winter seasons from October 2019 to February 2020, in the winter season between December 2020 and February 2021, as well as events in June 2019 and May 2021 (Fig. 4).

Leaky barrier inundation relative to channel bank height can be classified into five operational flow conditions for a typical leaky barrier at Wilde Brook (Fig. 5): (1) base flow through the gap under the leaky barrier with nil to minor backwater rise; (2) inbank flows obstructed by the barrier, with water flowing through the barrier and bottom gap; (3) overbank flows spilling onto one or both upstream floodplains prior to barrier overtopping; (4) overbank flows overtopping the barrier upstream; and (5) overbank flows with complete barrier submergence, with the relative magnitude of backwater rise decreasing with increasing downstream water level. In condition (5) for some cases, the downstream water level meets the upstream level, which coincides with inundation of both floodplains.

Unobstructed base flow and inbank flows (conditions 1 and 2) were the most prevalent, occupying 99.82%, 99.48%, 98.83% of the total record time, while overbank flows overtopping the barriers (conditions 3 and 4) occurred during the heavy rainfall and storm events for 0.184%, 0.517%, and 1.17% of the monitoring period for the Wilderhope Upper, Middle and Lower sites, respectively. A fully submerged barrier (condition 5) was observed once during Storm Dennis (15–16 February 2020) at the Wilderhope Upper and Wilderhope Middle sites, lasting for 2.5 h and 0.75 h, respectively.

The Wilderhope Middle leaky barrier developed significant scour underneath and on the downstream side of the structure, as shown in Fig. 7, which increased the flow area below the structure and prevented the downstream water level from reaching the upstream water level in the fully submerged barrier condition (condition 5) as often as the other monitored barriers, even though flows overtopped the barrier.

The Wilderhope Lower site barrier became fully submerged (condition 5) during the heavy rainfall on 25–26 October 2019 (see Table 3) and during the local storm on 14 Nov 2019, during Storm Dennis and Storm Christoph as well as during the rainfall event of 28 January 2021, for a total of 28.75 h, or 0.15% of the monitoring time. The flow depth at which the barrier was submerged in condition 5 changed over time, associated with formation of a hole on the left-hand side of the barrier next to the bank, which was observed during a site visit on 9 July 2021.

3.3. *Upstream relative to downstream submergence depths*

For all leaky barriers, the upstream sensor submergence depth increased relative to the downstream sensor submergence depth over the barrier vertical extent (Fig. 6a-c). The relative relationship between upstream and downstream depths differed between barriers and changed over time.

The depth recorded by the upstream sensor at the Wilderhope Upper site increased relative to the downstream sensor over the barrier vertical extent, with the upstream and downstream sensor submergence depth near $y = x$ (Fig. 6a, black dotted line) below the barrier lower edge. A change in curvature was associated with the barrier top vertical edge, due to flow overtopping the barrier (Fig. 6a, black solid line denoting barrier top edge). The relative increase in upstream relative to downstream sensor submergence depth over the barrier vertical extent increased over time (black, blue and cyan to red open circles), associated with accumulation of smaller logs, leaves, and brash upstream of the barrier, observed on photographs and measurements of the longitudinal barrier length, creating enhanced backwater effects.

At the Wilderhope Middle site, initial barrier construction consisted of a woven barrier extending from the channel bed to approximately 1 m above the bed. The relationship between upstream and downstream sensor submergence depth initially steepened following a period of steady rainfall, 25–26 October 2020 (Fig. 6b, black/blue to cyan open circles). The increase in upstream relative to downstream sensor submergence depth is consistent with accumulation of brash, leaves and fine material at the barrier. A change in this relationship (Fig. 6b, cyan to red open circles) was subsequently observed during Storm Dennis (16 February 2020). After this point, the downstream sensor submergence depth was greater than the upstream sensor submergence depth (Fig. 6b, $y = x$ indicated by black line) for low flows, with a relative increase in relative upstream–downstream relationship observed at higher flows. Photographs and survey observations recorded development of bedload transport immediately downstream of the barrier, with a limited region of scour pool initially present in February 2019, prior to installation of monitoring equipment. Over time, the downstream pool region increased in longitudinal extent, extending past the downstream sensor in July 2021. Bedload sediment removed from this pool was observed to

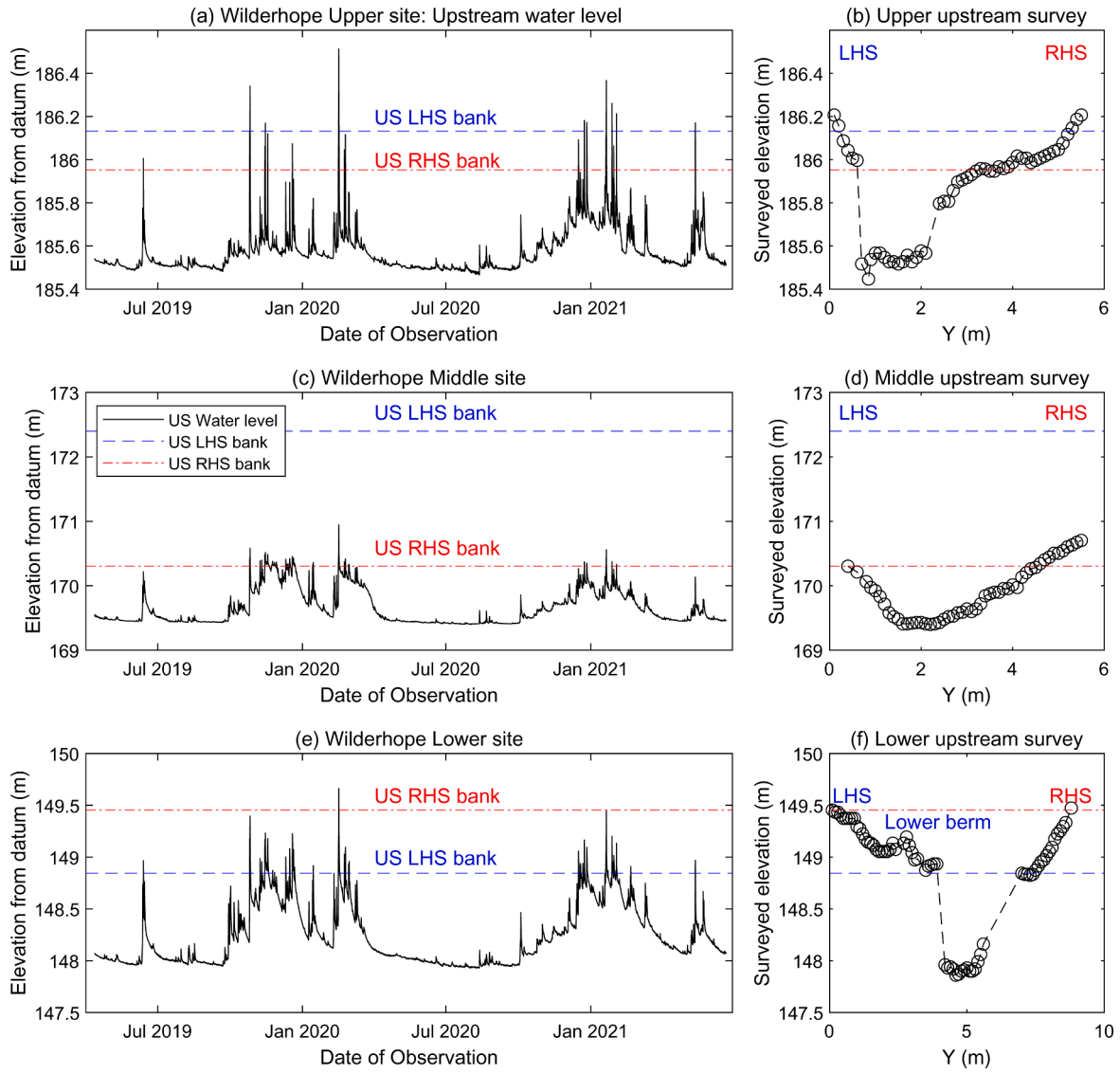

Fig. 4. Upstream pressure transducer sensor submergence depths at the (a) Wilderhope Upper, (c) Wilderhope Middle, and (e) Wilderhope Lower monitoring sites, with right and left bank levels indicated by dash dotted red and dashed blue lines, respectively, above which overbank flows occurred. Surveyed cross-sections at the location of the upstream pressure sensor (surveyed in November 2020) are shown on the right (b, d, f), with right- and left-hand side bank elevations indicated by dash dotted red and dotted blue lines. (For interpretation of the references to colour in this figure legend, the reader is referred to the web version of this article.)

accumulate and create an exit bar approximately 4 m downstream of the barrier. These changes in bed morphology are shown in Fig. 7. Following the change in relationship observed during Storm Dennis, a repeated decrease, increase, then decrease in relative upstream–downstream relationship was observed (Fig. 6b, red to pink, pink to green, green to yellow open circles) over time. In addition, the change in curvature associated with the top vertical edge of the barrier was less pronounced than the observations just prior to Storm Dennis (Fig. 6b, cyan open circles, 26 October 2019 to 16 February 2020). Compared to the Wilderhope Upper monitoring site, for which the top vertical edge of the barrier consisted of a substantial solid log, the upstream edge of the Wilderhope Middle barrier was composed of a woven arrangement of much smaller interlinked members (section 2.4), which was observed to be altered by the formation of a lateral gap in the barrier and bedload transport underneath the barrier over time, as shown in photographs of the barrier in Fig. 7.

At the Wilderhope Lower site, an increase in relative upstream–downstream depth relationship over the barrier vertical extent was initially observed (Fig. 6c, blue open circles). During Storm Dennis, the relative increase in upstream depth decreased relative to downstream sensor submergence depth (blue to black open circles). Over time, a sparser portion of the barrier adjacent to the LHS bank widened, creating a lateral gap between the barrier and the LHS bank.

The relationship between upstream and downstream sensor depths was observed to shift following storm events. Fig. 8 presents the backwater rise defined as the difference between the upstream (US) and downstream (DS) sensor depths, against the upstream sensor depths relative to the bank and barrier heights for storm events on 25–31 October 2019, and 16–19 February 2020, corresponding to approximately 4 yr return period events. The occurrence of each measurement point in the rising or falling limb of the storm hydrograph and relationship between upstream backwater depth and elevation of upstream channel banks and the barrier top edge are indicated by marker type and colour. The maximum recorded backwater rise was 0.49 m on 16 February 2020 at Wilderhope Upper, 0.80 m on 14 November 2019 at Wilderhope Middle, and 0.40 m on 14 November 2019 at Wilderhope Lower.

During the inbank condition of the hydrograph before the barrier and banks were overtopped (conditions 1 and 2), flows were characterised by an increase in US-DS difference with increasing US depth (open black

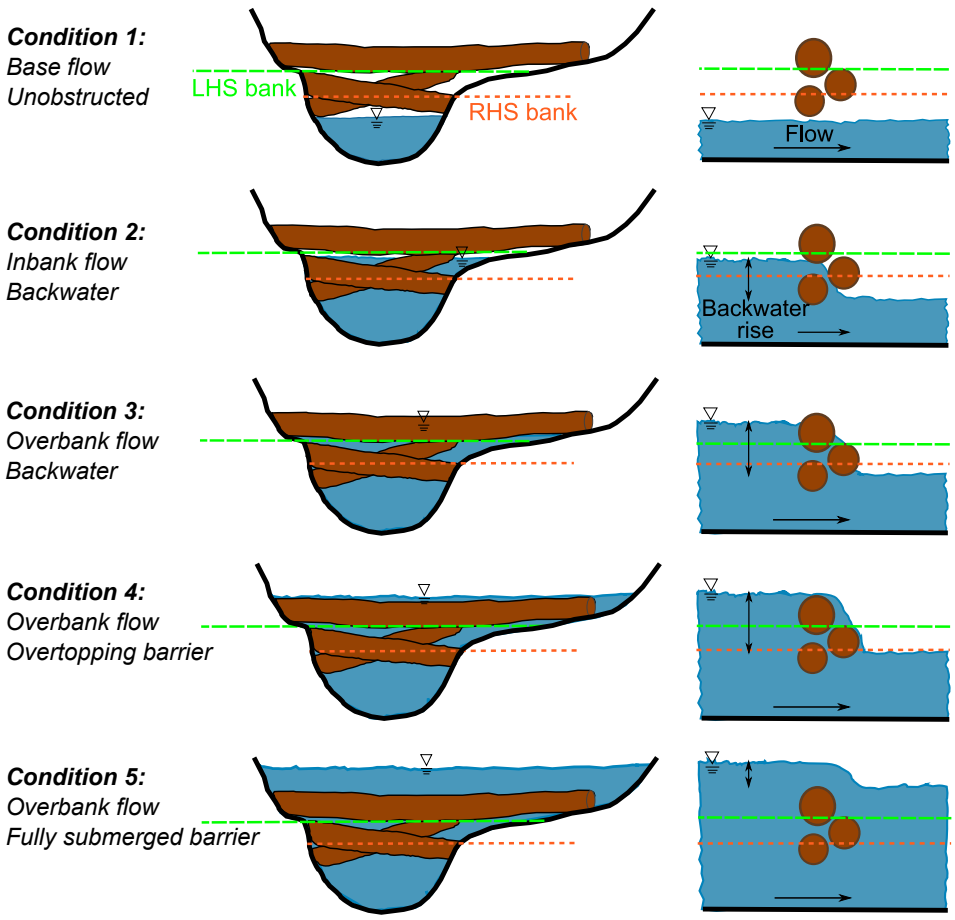

Fig. 5. Leaky barrier flow condition classified into five operational conditions relative to leaky barrier inundation and bank levels. Upstream cross-sectional view looking in the downstream direction is shown on the left and longitudinal profile view is shown on the right. Profile views indicate the backwater rise (black vertical arrow) as a function of the barrier submergence. LHS and RHS banks are indicated by green dashed, and orange dotted lines, respectively. Logs comprising the barrier are shown in brown, and the water surface is shown in aqua blue. Flow direction is indicated by black arrows. (For interpretation of the references to colour in this figure legend, the reader is referred to the web version of this article.)

circles and open blue squares), the rate of which changed when the flow transitioned to partial overbank mode, where the rate of increase of US-DS depth diminishes (condition 3; full black circles and full blue squares). As the water level reached the top spill height of the barrier, i.e., the barrier overtopping mode (condition 4; red plus sign markers), the relative backwater difference decreased with increasing upstream depth, indicating that the upstream flow inundated the floodplains, while the downstream depth similarly increased due to flow spilling over the barrier (Fig. 8).

In the falling limb of the storm hydrograph after the water level had fallen below the barrier top edge (blue markers), a similar pattern was observed to the hydrograph rising limb (black markers), with the exception of Storm Dennis in February 2020. During this event, the US-DS difference remained steady with increasing US depth, indicating that the backwater rise of Wilderhope Middle (Fig. 8d) and Wilderhope Lower (Fig. 8f) barriers was matched by a similar rate of change of the downstream water depths. This could be due to the formation of a deeper scour hole, and washout of brash and leafy material following overtopping of the barrier for the Wilderhope Middle site, and formation of a lateral gap between the barrier and bank at the Wilderhope Lower site during Storm Dennis.

For several storm events, temporal shifts in the relative US and DS water level relationship described in section 3.3 were also observed in the relationship of backwater rise with US sensor depth (Fig. 8) and flow rate (Fig. 9), particularly amongst the October, November, and February 2020 storms. For the Wilderhope Upper barrier, for a given discharge there was a maximum net increase in backwater rise of 0.49 m on 13 February 2020, following Storm Ciara (08–09 February 2020) attributed to barrier accretion. While for the Wilderhope Middle barrier following the ~ 4 yr event on 25–31 October 2019, at lower flows a decrease in net backwater rise accompanied the falling limb of Storm Brendan (13–16 January 2020) linked to barrier depletion. Subsequent storm events, Storm Ciara and Storm Dennis, showed similar reduced peak and falling limb backwater rise than previously observed, associated with depletion. Similarly, at Wilderhope Lower barrier, the higher backwater rise was observed following the 4 yr return period event in October 2019 was reduced during similar flows in the December 2019 events, Storm Atiyah and the 1.7 yr event on 18–31 December 2019.

Due to accretion and depletion of material from the structure, barrier performance and backwater rise changed cyclically following storm events (Fig. 9, from blue, green to yellow data series in Fig. 6. At Wilderhope Middle for instance, for similar flow during the 25–31 October 2019 event, peak backwater rise for the 13 November 2019 event was increased by a factor of 1.9, however, depletion of the barrier diminished backwater rise to a factor of 1.2 by 27 February 2020 after Storm Dennis (Fig. 9). The cyclical change in backwater rise observed for the Wilderhope Middle and Lower barriers was not observed for the Wilderhope Upper barrier, which saw an increase in backwater rise for a given discharge without diminishing over time (Fig. 9) likely due to the cross-section profile and two log structure at Wilderhope Upper (Table 1), where accumulated material became lodged and trapped between the two logs.

Over time, accretion of wood material and sediment, and depletion of the barrier structure is therefore linked to the storms affecting the rate of rising of the upstream depth relative to the downstream depth (Fig. 6). Differences in the rising and falling limbs of the storm hydrograph may also demonstrate that the storms physically changed barrier structure, for instance the falling limb being lower than the rising limb curve for the Wilderhope Upper site (Fig. 8a) while the opposite was observed for Wilderhope Middle (Fig. 8c), during the October 2019 event.

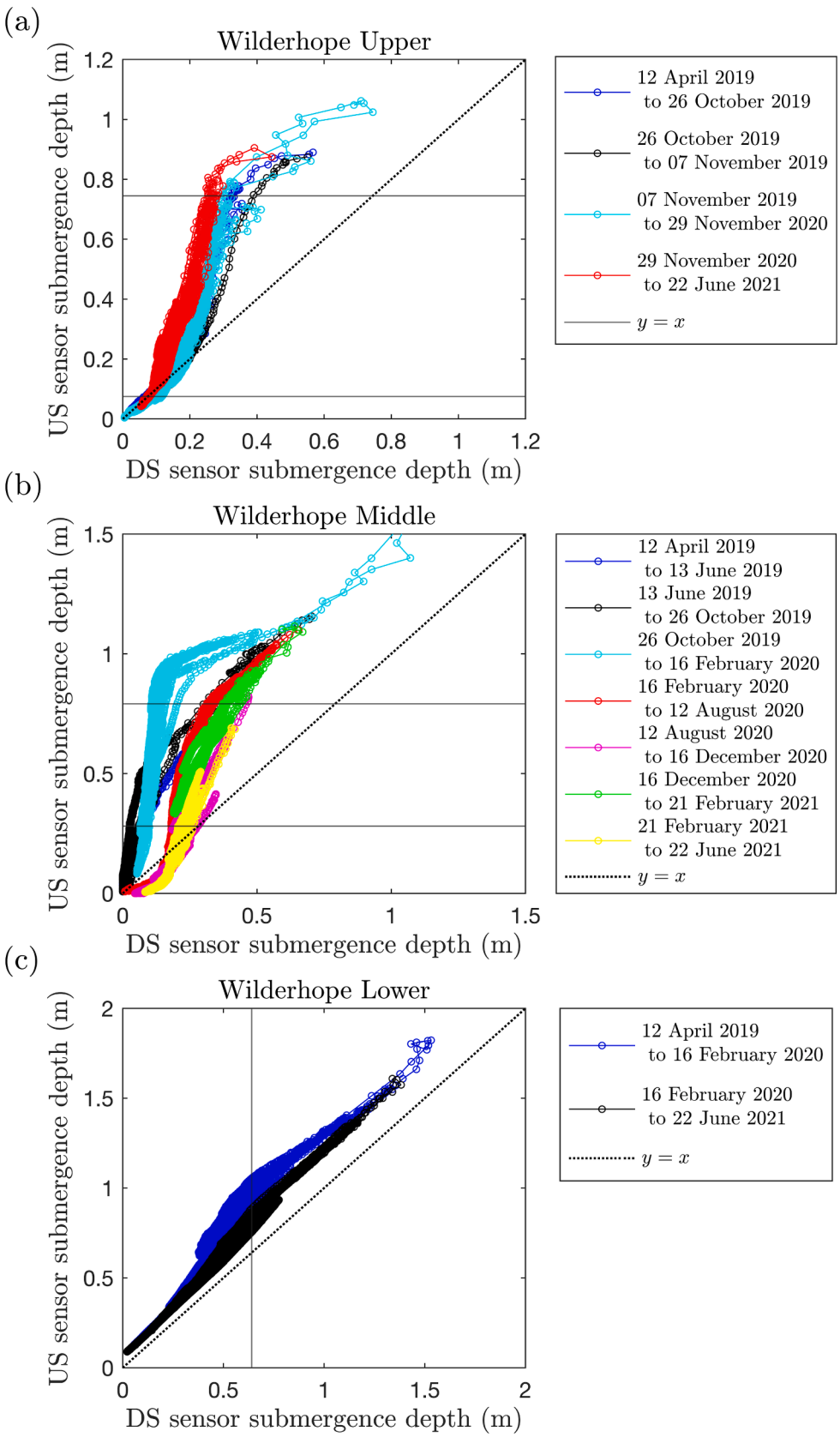

Fig. 6. Recorded concurrent upstream pressure transducer sensor submergence depth relative to downstream sensor submergence depth (open circles), for monitoring sites (a) Wilderhope Upper, with centre top of the barrier in September 2021 indicated by the horizontal black line, (b) Wilderhope Middle, centre top of the barrier indicated by horizontal black line and bottom of gap formed within the barrier (0.25 m), recorded in September 2020, indicated by horizontal black line, and (c) Wilderhope Lower, with centre top of the barrier measured from the downstream face of the barrier indicated by vertical black line. Line of equality $y = x$ shown by dotted black line.

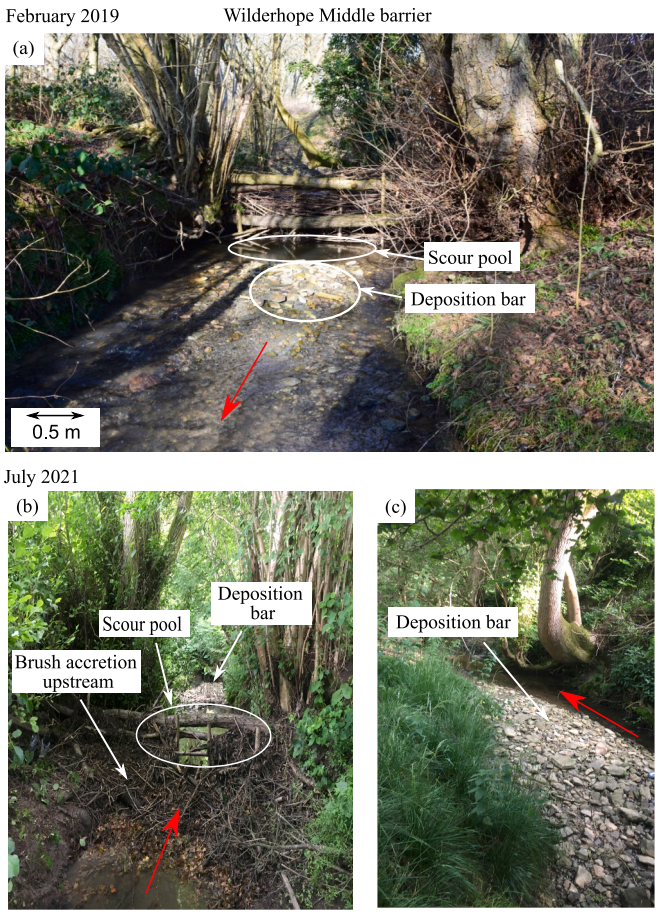

Fig. 7. Photographs of the Wilderhope Middle barrier showing local bathymetry changes from bedload scour and deposition downstream of the barrier from (a) February 2019, and to (b) and (c) in July 2021. Photos show reach immediately the downstream of the barrier in (a) and (c),) and upstream of the barrier in (b), which also shows brash accumulation upstream of the barrier and the formation of a gap within the barrier structure.

3.4. Storage volumes

The meshgrid interpolated from SfM DEM bathymetry data are shown in Fig. 10a, with locations of leaky barriers in the surveyed subreach indicated. The area upstream of the Wilderhope Lower barrier, up to the next upstream barrier, for which the volume was integrated is outlined (Fig. 10a, dashed red line). The volume of water stored in the area upstream of the Wilderhope Lower barrier was estimated using DEM and Lidar bathymetries (Section 2.6). The difference between Lidar and DEM generated volumes decreased with increasing water depth (for $H \leq 0.68$ m volume difference ranged between 25 and 31%, and for $0.71 < H < 0.86$ m volume difference was $<$ 20%). Visibility of the channel bed and bank, and the spatial resolution difference are contributing factors to these differences, as the water surface, vegetation and tree canopy cover reduces the precision of the Lidar measurement (Su and Bork 2006, Javernick et al., 2014).

The total water volume (V) shown in Fig. 10b was estimated by assuming a horizontal water surface level at the elevation recorded by the upstream pressure transducer. The net water volume (V_n) (Fig. 10c) was found from the difference between the water volume calculated using the upstream pressure transducer water elevation and that calculated using the downstream pressure transducer water elevation. Fig. 10b shows the total storage volume and (c) the slope change of the total volume relative to the water depth, with levels corresponding to ~ 2 yr and 4 yr return periods indicated. The total volume increased with increasing water depth, and no abrupt changes in volumes were associated with inundation of the different bank and berm levels (Fig. 10c). Bankfull storage volume upstream was estimated around 80 m^3 and peak volume was 320 m^3 for the 16 February 2020 event (~4 yr return period).

The peak net volumes occurred during the highest flow magnitudes observed. Return periods of around 2 yr on 19 December 2019 and 14 November 2019, and 4 yr on 26 October 2019 and 16 February 2020 are shown in Fig. 11b. The associated water volume storage ranged between 52 to 56 m^3 for the 2 yr return period events, and between 56 and 102 m^3 for the 4 yr return period events for the Wilderhope Lower barrier, with the difference attributable to the uncertainty in the discharge derived from the rating curve having a standard error of 0.0271 m^3s^{-1} and differences observed in water levels at the Wilderhope Lower barrier and the Flow Site velocity sensor. The peak water level recorded at the Flow Site velocity sensor site during the 26 October event was only 0.009 m less than that recorded during the 16 February 2020 event, which gave both events an estimated return period of 4 yr. For both these events, recorded peak water levels at the Flow Site velocity sensor (H = 1.08, 1.09 m for October 2019 and February 2020 respectively) were close to the measured culvert height of 1.1 m. However, at the Wilderhope Lower site, the upstream water level during the October event was 0.266 m less than the February event, which resulted in different storage volumes (Fig. 11 (b)).

Time series of the difference between upstream and downstream depths compared to the net storage volume (Fig. 12b and e) with rainfall intensity (Fig. 12a and d) and upstream cross-sectional average velocity and corresponding event discharge at the Flow site velocity sensor (Fig. 12c and f) are shown in Fig. 12 for the October 2019 and February 2020 storm events. During the storm rising limb, the increase in backwater rise corresponded to an increase in net storage volume. Following the transition of flow conditions from inbank to overbank and overtopping of the barrier, the rate of increase of net storage volumes was lessened by the decrease in relative US-DS difference. The net storage volume (V_n) gradually decreased during the receding limb of the hydrographs as the barriers gradually released water, with the exception of the prolonged rainfall event starting on 13 November 2019, where two low discharge events occurring in close succession resulted in coalescing net storage that remained throughout a 6-day period. The sudden dip in upstream cross-sectional velocity at the start of the rising limb, indicates the commencement of overbank flow, as the flow inundates the banks and area increases at a greater rate than the increase in discharge (Fig. 12c and f). This is followed by a sudden rise in velocity as the discharge rises as the surface runoff volume increases, and levels of high discharge are maintained, represented by a series of peak flows in the hydrograph. After the flow recedes, the upstream velocity remains lower than the 'before' condition as the upstream storage provided by the leaky barrier is slowly released downstream over several days (Fig. 12b and e).

4. Discussion

4.1. Data uncertainties

The results presented here are from the monitoring of a small catchment (5.3 km^2) and small stream, with a focus on paired pressure transducer gauged barriers. *In-situ* instrument battery problems caused gaps in flowmeter data, limiting the duration over which the discharges were evaluated. Available flow data was extrapolated using a rating curve to obtain discharges for a period where the Flow Site velocity sensor had logged erroneous data. The use of a rating curve derived from a short record length is a potential source of uncertainty in flow determination, together with the application of a FEH method for estimating the return period for small catchments ($<$25 km^2) (Faulkner et al., 2012). In addition to catchment and stream size specific results, various leaky barrier designs also perform differently as indicated by the Wilde brook barriers interacting with the flow according to their properties,

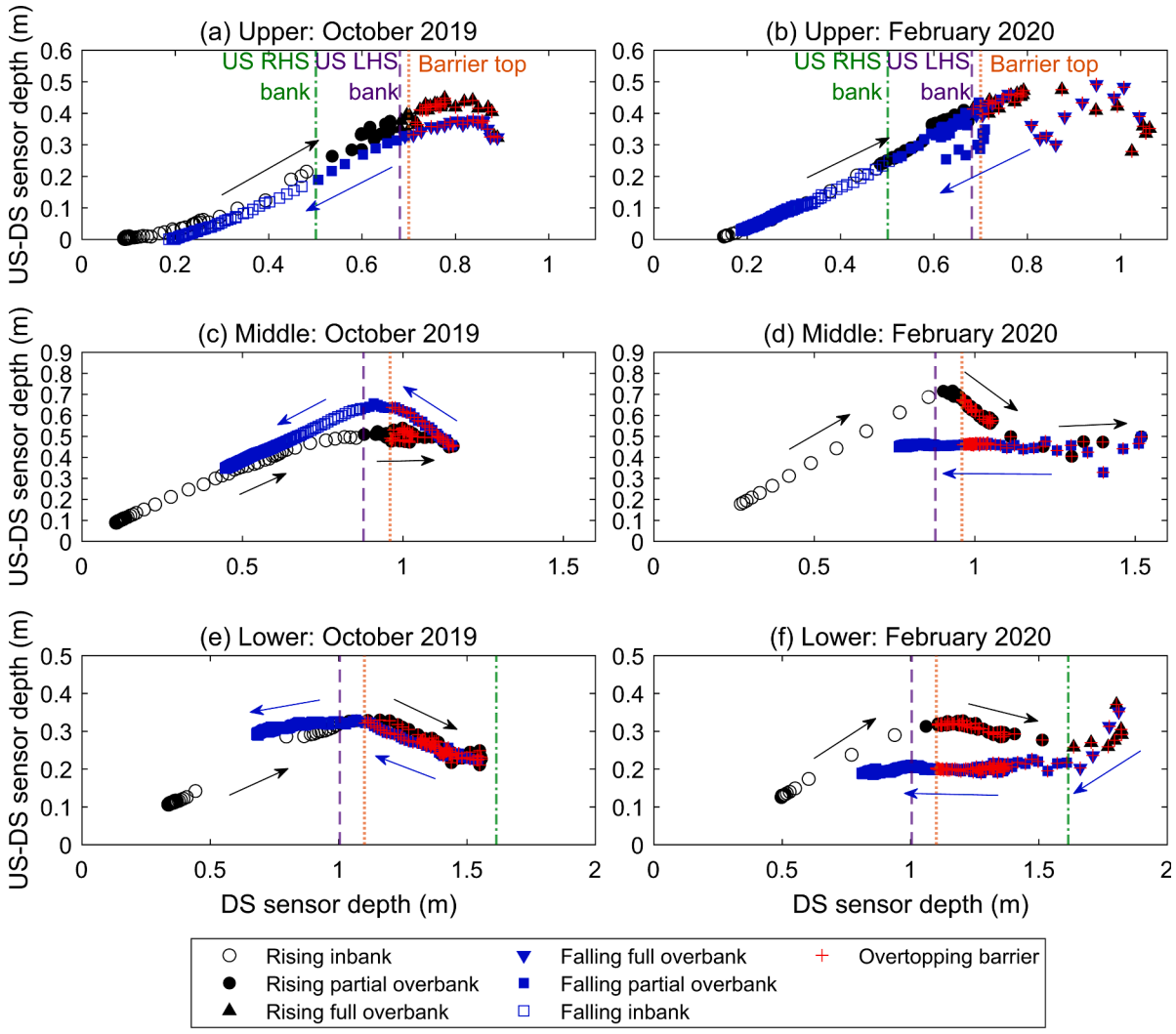

Fig. 8. Backwater rise, upstream (US) minus downstream (DS) sensor depth, against US sensor depth for the Wilderhope Upper (a,b), Wilderhope Middle (c,d) and Wilderhope Lower (e,f) barriers during the October 2019, and February 2020 storm events. The rising (black markers) and falling (blue markers) of the storms are shown, with overtopping of the barrier indicated (red plus sign). Arrow annotations indicate the rising (black) and falling (blue) limbs. Upstream bank levels on RHS (green dash dot line) and LHS (indigo dashed line), and the top of the barrier (orange dash dot line) are indicated. (For interpretation of the references to colour in this figure legend, the reader is referred to the web version of this article.)

local channel profile and location within the catchment.

4.2. *Comparison of the paired barriers, local impact on overbank flows*

The hydraulic response to the observed storm events varied amongst the barriers with paired pressure transducers. The observed frequency of overbank flows depended on the local channel cross-sectional profile including the elevation and steepness of the banks and berm, which differed at the three measurement sites (Fig. 44b, d and f). The Wilderhope Upper (Fig. 4b4) and Wilderhope Lower (Fig. 4f4) sites follow compound channel profiles, while the Wilderhope Middle (Fig. 4d4) site resembles an incised channel with steep banks. Incised channels are typical of upper catchment streams where leaky barriers have been installed in previous case studies (Burgess-Gamble et al., 2017). The occurrence of overbank events (Fig. 44) and the response of each barrier varied according to the barrier design and channel characteristics including the presence and extent of the barrier lower gap, log number, diameter, and spacing, barrier vertical extent, channel bankfull depth and width, and local bathymetry. In addition, barrier impact on backwater rise varied over time due to accretion and depletion of logs, brash, and leaves comprising the barriers, and local scour at the channel bed (Wilderhope Middle) and sides (Wilderhope Lower). The increase and decrease in backwater rise over time is similar to that observed by Geertsema *et al.* (2019), where the local channel profile and type of wood patch also impacted backwater effects. The highest magnitude backwater rise of the three monitored barriers was observed for the Wilderhope Middle barrier (Fig. 9), which was located in a confined channel section with an 0.7 m barrier vertical extent and, at installation, no lower gap (Fig. 2c). A small lower gap extent (0.05 m) relative to the channel bankfull depth developed following installation (Table 1). At Wilderhope Upper, the backwater rise increased with time (Fig. 9a, blue to yellow series), associated with accumulation and entrapment of small logs, leaves and sediment (Fig. 2a), but the magnitude of backwater rise remained lower than that observed at Wilderhope Middle most likely due to the Upper's lower channel cross-sectional area and shallower vertical extent (0.47–0.5 m, Table 1). Backwater rise reduced at the Wilderhope Lower site following Storm Dennis, linked to development of a lateral gap due to local scour at the channel sides. To maximize backwater rise, a leaky barrier should extend over the full channel section in a deeper, confined reach. A small lower gap vertical distance increases the longitudinal velocity in the gap region and likelihood of sediment transport below the barrier, generating a downstream scour pit

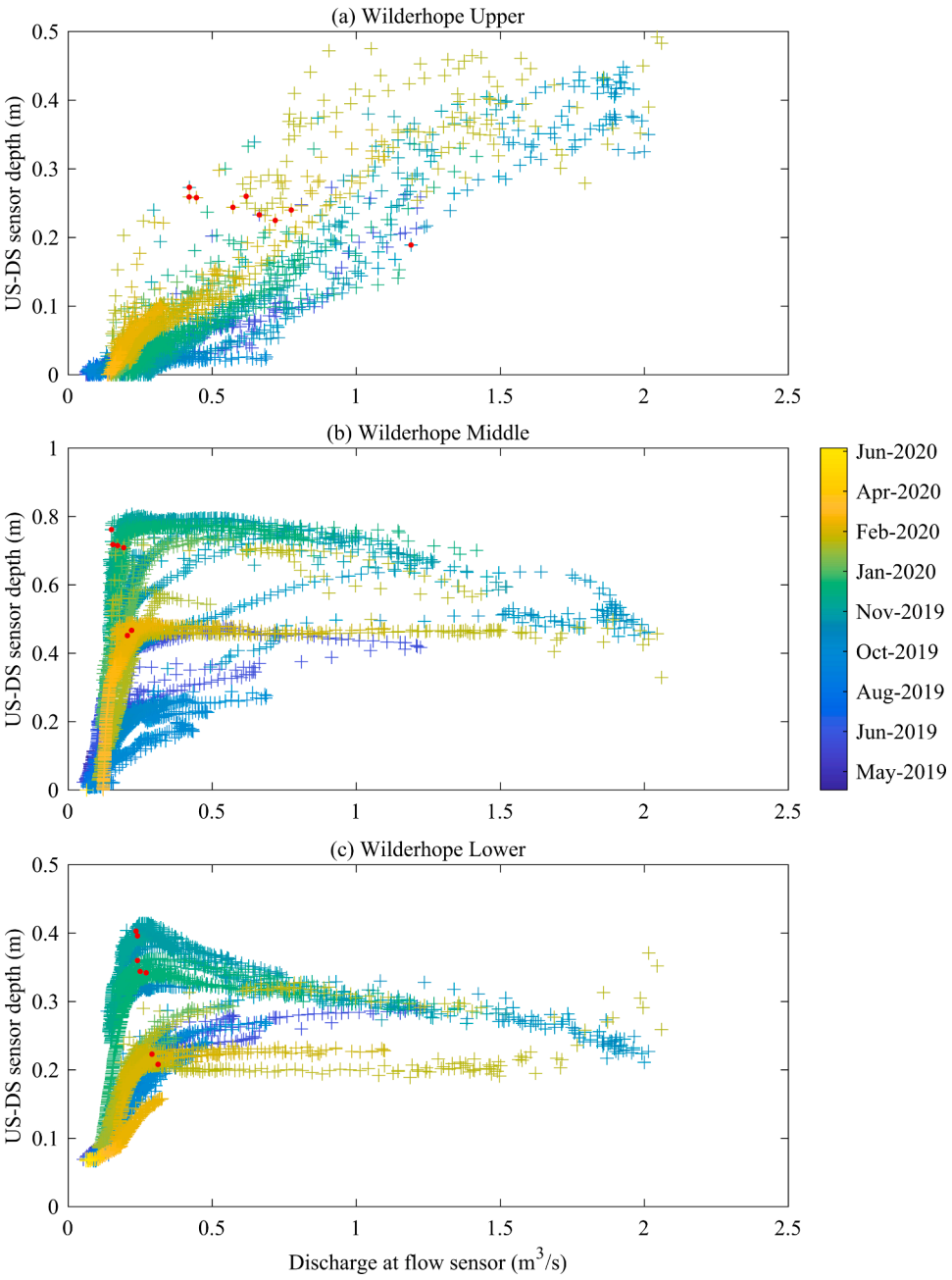

Fig. 9. Backwater rise upstream (US) minus downstream (DS) sensor depth, against the discharge at the Flow Site velocity sensor for the Wilderhope Upper (a), Wilderhope Middle (b) and Wilderhope Lower (c) barriers for the monitoring period spanning from May 2019 to June 2020. Red circle markers indicate backwater rise corresponding to initial occurrences of bankfull conditions. (For interpretation of the references to colour in this figure legend, the reader is referred to the web version of this article.)

as at the Wilderhope Middle site (Follett et al. 2021). A larger lower gap reduces likelihood of local bedload transport, but also reduces barrier vertical extent and maximum backwater rise. The possibility of accretion and depletion of barrier material and potential for local sediment transport should be considered when locating barriers, with barriers situated away from river infrastructure such as culverts, bridges, and road crossings.

At Wilde Brooke the bed slope was moderate ($S_0 \sim 0.01$, Digimap). Observed bedload scour was associated with a deposition bar immediately downstream of the scoured area. A barrier located downstream of the deposition area may have reduced further bedload transport of scoured sediment. Care should be taken when considering barrier placement and potential sediment transport at sites with significantly milder or steeper slope.

The temporal changes in backwater differences for various storms were reflected in the relative upstream and downstream sensor depths for the three barriers. During barrier overtopping, the downstream depth increased while the US-DS difference decreased, indicating that the upstream depth rate of increase was lower than the downstream, with the exception of Storm Dennis in February 2020 (Fig. 8). The falling limb of Storm Dennis showed nearly constant difference in US-DS depth, probably due to changes in structural composition of the barriers following barrier overtopping. Depletion of material from the barriers likely occurred at the peak discharge, as physical gaps within the Wilderhope Middle and Wilderhope Lower barriers were observed in July 2020. A barrier design comprising two or more members, present at all three monitoring sites, allows flow through the barrier and encourages the trapping and lodging of debris between the gaps. This results in accretion of barrier solid volume from locally occurring material (Fig. 2), for no additional material and construction cost.

The reduction in cross-sectional velocity at cross-sections immediately upstream and downstream of three monitored leaky barriers are shown here (Fig. 12). However, the cumulative effect of the 105 barriers on the flood peak reduction and peak time lag requires further

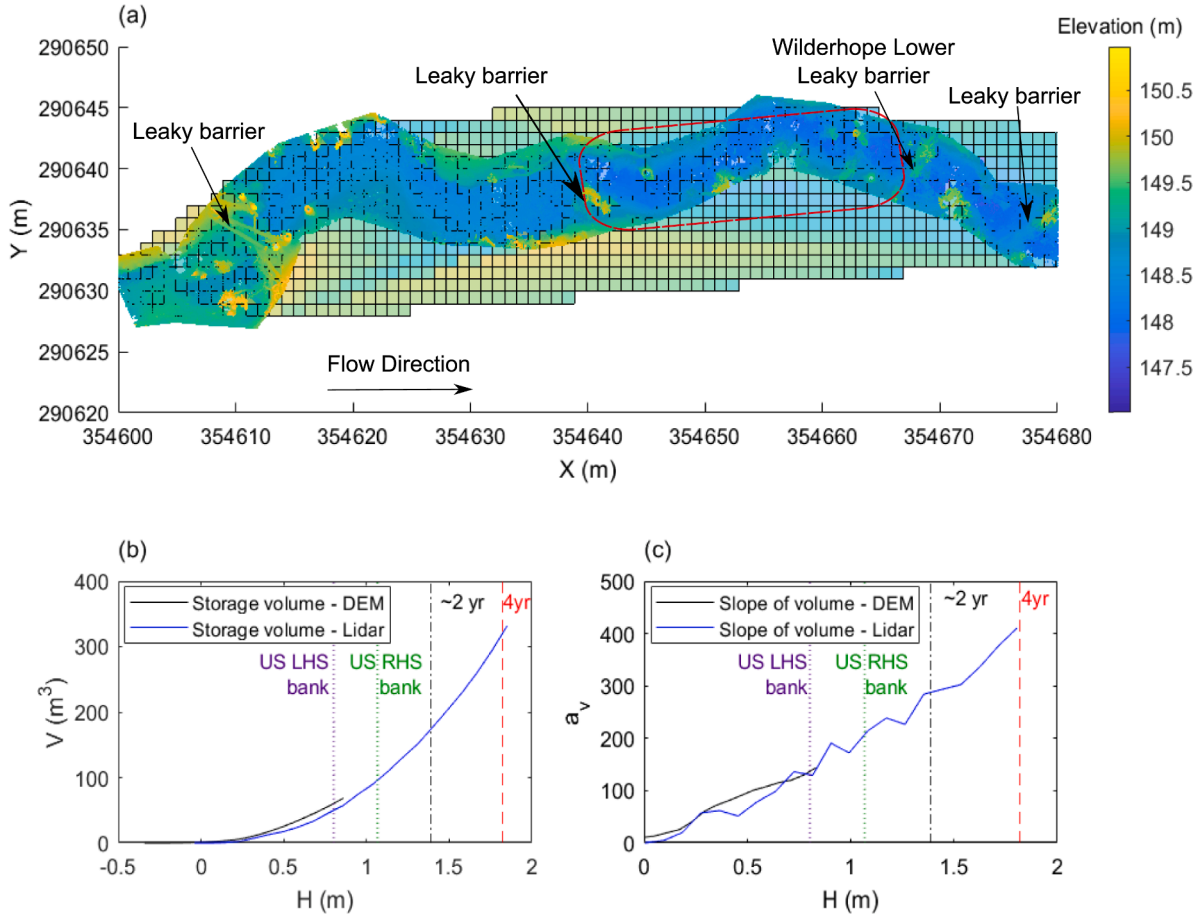

Fig. 10. (a) DEM and meshgrid of the Wilderhope Lower subreach, with the red dashed line outlining the area for which the volumes are calculated; (b) total volume V (DEM: full black line, Lidar: full blue line) relative to the upstream pressure transducer depth H at the Wilderhope Lower monitoring site; (c) the slope a_v (DEM: full black line, Lidar: full blue line) of the total volume V - flow depth relationship (shown in Fig. 10b). Purple and green dashed lines indicate the left-hand and right-hand side bank levels, respectively. (For interpretation of the references to colour in this figure legend, the reader is referred to the web version of this article.)

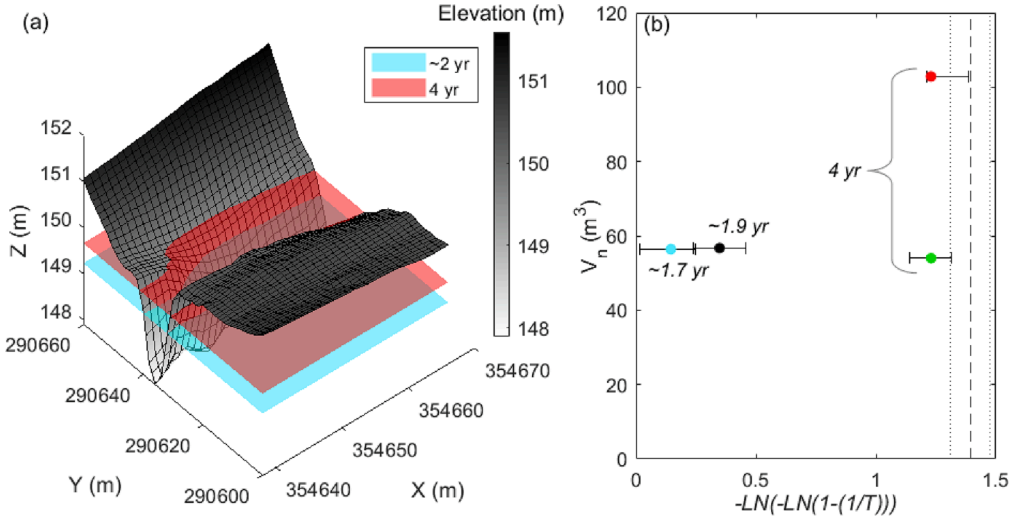

Fig. 11. (a) 2 m Lidar bathymetry of the area upstream of the Wilderhope Lower barrier for which the volumes were calculated, with surfaces indicating inundation levels for an approximately 2 yr return period event of 19 December 2019, and the 4 yr return period event Storm Dennis on 16 February 2020. (b) Peak net storage volume V_n for the two events shown using Lidar bathymetry in (a) and the ~ 2 yr event on 14 November 2019 and 4 yr event on 26 October 2019. Horizontal error bars represent the standard error in the return period estimated from the rating curve derived discharge (See section 2.2). Vertical dashed black line indicate the return period corresponding to the maximum depth of the culvert at the Flow Site velocity sensor, and vertical dotted gray lines indicated the lower and higher standard errors for the return period estimate based on this depth, respectively,

consideration, and because there is no "before" data available this will be investigated in a future modelling study of the Wilde Brook test reach.

4.3. Temporal changes in barrier physical properties

Temporal changes in relative upstream and downstream sensor depths at the three measurement sites are shown in Fig. 6. River wood

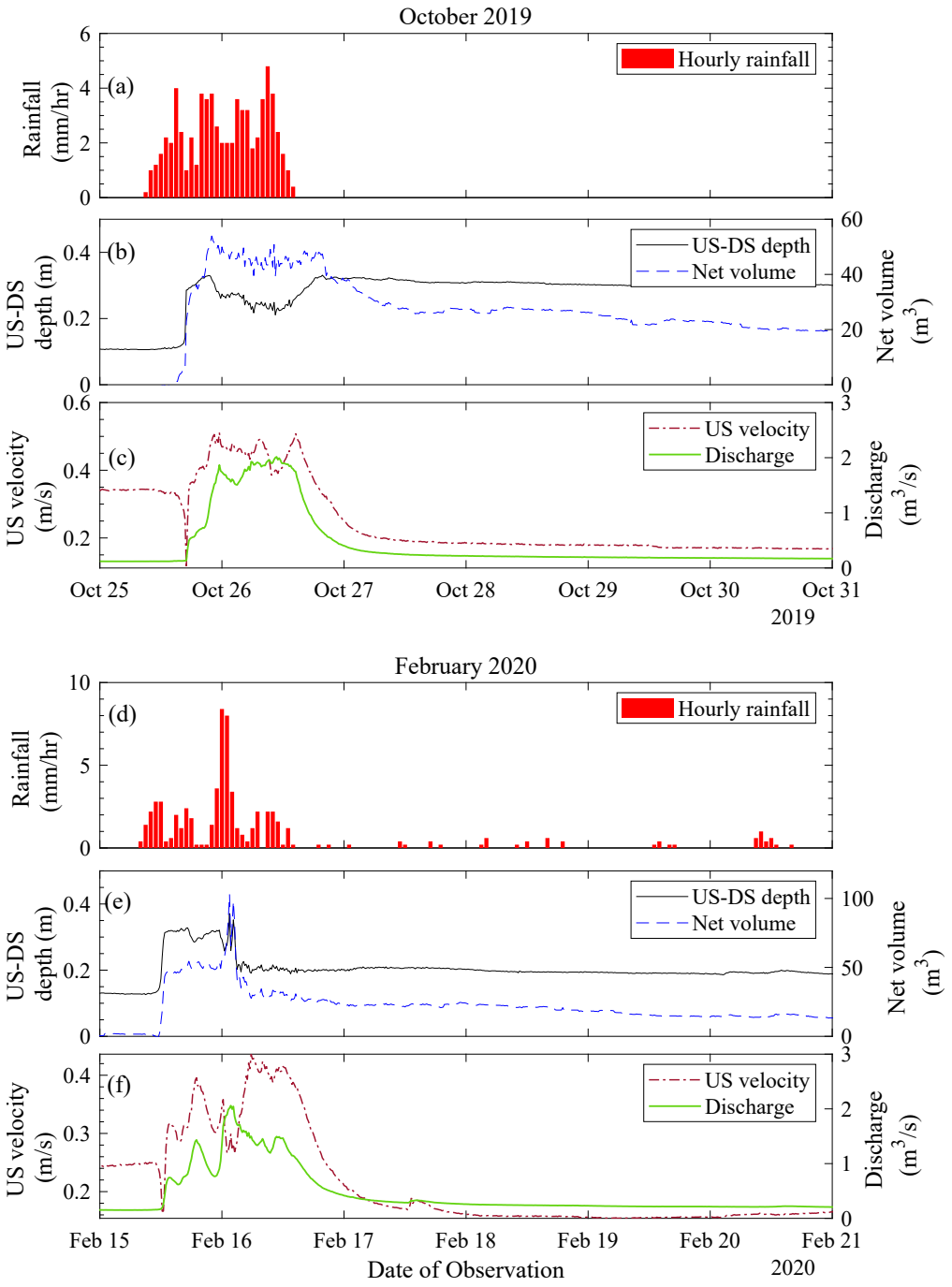

Fig. 12. Rainfall, difference between upstream (US) and downstream (DS) water depth (black line, right axis) and Net storage volume V_n (blue dashed line, left axis) over time for the Wilderhope Lower barrier, calculated using Lidar bathymetry, and upstream cross-sectional average velocity (red dash-dot line, right axis) and discharge Flow site velocity sensor (green full line, left axis) for storm events October 2019 (a, b, c),and February 2020 (e, f, i). The horizontal axis is set at the same scale (6-day period) for each event. (For interpretation of the references to colour in this figure legend, the reader is referred to the web version of this article.)

availability is subject to seasonal change in riparian vegetation and wood recruitment and transport along the river (Ruiz-Villanueva et al., 2016), temporally affecting the barrier composition. Accumulation of brash and leaves mobilised and deposited by runoff following heavy rainfall and storm events, followed by wash out or depletion due to decay, change the barriers' physical structure, affecting barrier composition and backwater effect (Dixon 2016; Pinto et al., 2019). Bedload transport and channel bed changes were observed through photographic records, particularly at the Wilderhope Middle site, where a bed scour hole developed and deepened over time. Addy and Wilkinson (2016) also observed localised sediment scour and accumulation around engineered log jams, and woody debris and vegetation displacement following a storm event, indicating that storms impact barrier physical composition. The relative water depth relationship upstream and downstream of the barriers also likely influenced bedload transport, as the presence of a lower vertical gap increases near-bed streamwise velocity, bed shear stress, and Shields parameter, or dimensionless shear stress found from ratio of hydrodynamic forces to submerged particle weight, relative to conditions for an unobstructed channel (Schalko et al., 2019; Follett and Wilson, 2020, Follett et al. 2021). As conditions approach the critical threshold, the likelihood of bedload sediment transport increases (Garcia et al., 2000; Julien, 2010). As the vertical gap distance increases relative to bankfull depth, the increase in longitudinal velocity and bed shear stress is reduced (Follett et al. 2021).

4.4. Storage volume

To evaluate the water storage generated by the leaky barrier, the upstream volumes above the bed were estimated for a given water level. The assumption of a horizontal water surface in the trapezoidal integration calculation of water volume was a likely source of uncertainty, underestimating the true storage due to omission of volume due to water surface gradient. Similar to the relative water level rise between upstream and downstream of the barrier being governed by the barrier properties and channel profile, the net storage volume is also governed by these factors. Hence, an increase in backwater rise (Figs. 4 and 5) following accretion of material likely results in increased storage volume. For instance, whilst both October 2019 and Storm Dennis in February 2020 were estimated to be of similar peak discharge, at their peak Storm Dennis showed more net storage than the October event (Fig. 11) due to greater backwater rise at the Wilderhope Lower barrier. The results from both high-resolution DEM and 2 m Lidar were consistent despite differences in resolution and precision, demonstrating that verified Lidar data may be used to approximate storage volumes gained by leaky barriers where high resolution bathymetries are unavailable. However, leaky barriers can lead to geomorphic changes, causing bathymetry to change over time, such as developing scour pools and riffles (Addy and Wilkinson 2016.; Burgess-Gamble et al., 2017). Therefore, we note that DEM and Lidar bathymetries only provide a single measurement of a temporally changing river.

The overall net volume increase for the 105 leaky barriers on the Wilde Brook test reach ranged between ~ 5,900 and 10,7007 m^3 for a ~ 4 yr return period storm event, which was based a volume of 56 m^3 and 102 m^3 per leaky barrier observed for the Wilderhope Lower barrier. Storage volumes estimated from other NFM monitoring studies vary widely due to differences in the scheme and setting, and the only other quantitative field-based study available gives a volume of 48 m^3 per leaky barrier which was evaluated for a reach with 35 leaky barriers from water levels and photographic records (Barnes, 2018).

Modelling studies evaluating storage volumes associated with leaky barriers often use lumped storage estimation methods from multiple runoff attenuation features and other NFM interventions for whole catchment, without quantifying the net leaky barrier storage per barrier. Maximum additional storage volume was computed as 70,000 m^3 for 59 leaky barriers, with individual barriers storing between 1,500 and 5,000 m^3 "total" volumes in a 29 km^2 catchment by Metcalfe et al. (2017). Hankin et al. (2020) modelled "maximum" barrier storage volumes for various leaky barrier numbers along a reach ranging from 245 m^3 to 457 m^3 for 10 to 20 leaky barriers in a subcatchment of < 0.5 km^2. Comparing leaky barrier storage volumes across modelling case studies is difficult due to different metrics used in volume reportage (e.g. total, maximum), and return period estimation uncertainty and more field and evidence-based studies are needed to elucidate leaky barrier storage performance from a range of different stream/catchment settings.

5. Conclusions

Field based monitoring on an NFM test reach with 105 leaky barriers was conducted over two years using a raingauge, a flow meter and paired pressure loggers upstream and downstream of three leaky barriers of varying design, cross-sectional profile, and bank and berm levels. The leaky barriers generated backwater rise which varied depending on the design and storm event magnitude. Events ranged from heavy rainfall to named storm events and featured storms up to return periods of approximately 4 yr (26 October 2019 and 16 February 2020). Floodplain inundation was influenced by storm magnitude, barrier and channel properties. Temporal shifts in relative backwater rise were observed to follow changes in leaky barrier physical properties and composition, where accretion of wood material on the barrier increased backwater rise, and depletion of material from the barrier decreased backwater rise. The maximum recorded backwater rise at three barriers ranged from 0.4 m to 0.8 m during ~ 2 and 4 yr return period events. Barrier accretion increased the maximum backwater rise by factors of 1.3 to 1.9 compared to the 26 October 2019 event, and barrier performance and resulting backwater rise changed cyclically following subsequent storm events. Additionally, bedload transport reduced changes in relative upstream and downstream depths, and the incidence of barrier overtopping. Using high resolution DEM, 2 m Lidar and recorded water levels, upstream storage and net storage volumes were calculated, showing that the bankfull storage volume upstream of the Wilderhope Lower barrier amounted to 80 m^3 while net storage increase was 52 m^3 during<2 yr return period events, and up to 102 m^3 during the 4 yr return period event, which translates to ~ 5,900 and 10,700 m^3 net volume increase for the 105 leaky barriers on the Wilde Brook test reach for a ~ 4 yr return period storm event. Backwater rise, cross-sectional average velocity, and net storage hydrographs showed rapid filling of the barriers in the rising limb, and in the falling limb the upstream velocity remained lower than the 'before' condition as the upstream storage provided by the leaky barrier was slowly released downstream over several days.

This study's findings indicate that to maximise the magnitude of backwater rise, leaky barriers should have a large vertical extent and be located in deeper, confined cross-sections along a stream reach. Where a lower gap is present, reducing it so that members extend over at least half of the channel depth enhances backwater rise, water storage and reduces longitudinal velocity over the backwater region. Designs composed of two or more members are effective at trapping material, resulting in 'natural' barrier accretion, thus increasing backwater rise and water storage performance at no additional material and construction cost. The potential for development of local scour, leading to gaps between the barrier and bed or barrier and channel sides, should be considered in light of site sediment management goals and barrier location. Although a larger lower gap reduces the likelihood of initiation of bedload sediment transport, this design also reduces the barrier vertical extent and magnitude of backwater rise.

This study provides quantitative field-based evidence on backwater rise, velocity reduction, and storage, which can inform current and future leaky barrier implementations. In addition, it provides new information for developing generalised approaches for representing leaky barriers in flood models. Monitoring of the site is ongoing to further evaluate the leaky barrier performance, temporal evolution, backwater, storage increase, and flood peak attenuation for additional wider ranging storm magnitudes.

CRediT authorship contribution statement

Valentine Muhawenimana: Methodology, Data curation, Formal analysis, Writing – original draft, Writing – review & editing. **Elizabeth Follett:** Methodology, Data curation, Formal analysis, Funding acquisition, Writing – review & editing. **Ian Maddock:** Data curation, Writing – review & editing. **Catherine A.M.E. Wilson:** Conceptualization, Methodology, Data curation, Funding acquisition, Resources, Writing – review & editing.

Declaration of Competing Interest

The authors declare that they have no known competing financial interests or personal relationships that could have appeared to influence the work reported in this paper.

Data availability

Data will be made available on request.

Acknowledgements

This project was part-funded by 'The Shropshire Slow the Flow

Natural Flood Management Project' DEFRA 2018 Monitoring Programme, and was conducted in partnership with Shropshire Council, Shropshire Wildlife Trust, the Environment Agency, WSP and the National Flood Forum. The first author was funded from the EPSRC Impact Accelerator Award and the European Regional Development Fund through the Welsh Government Sêr Cymru program 80762-CU-241. The second author was funded from Royal Academy of Engineering's Research Fellowships program and the European Regional Development Fund through the Welsh Government Sêr Cymru program 80762-CU-241.

References

Addy, S., Wilkinson, M., 2016. An assessment of engineered log jam structures in response to a flood event in an upland gravel-bed river. Earth Surf. Process. Landforms 41, 1658–1670. https://doi.org/10.1002/esp.3936.

ADEPT. (2019). Assessing the Risk: Assessing the Potential Hazards of using Leaky Woody Structures for Natural Flood Management. The Association of Directors of Environment, Economy, Planning and Transport (ADEPT). 190521-Assessing-the-risk.pdf (catchmentbasedapproach.org).

Arnott, S., Burgess-Gamble, L., Dunsford, D., Webb, L., Johnson, D., Andison, E., Slaney, A., Vaughan, M., Ngai, R., Rose, S., Maslen, S., 2018. Monitoring and evaluating the DEFRA funded Natural Flood Management projects. Technical Report: Environment Agency, 20 July 2018. Available https://catchmentbasedapproach.org/wp-content/uploads/2018/11/NFM-MonitoringObjectivesFINAL-v18.pdf.

Barnes, M.S., 2018. Assessing the potential for forest-related natural flood management to mitigate flooding. Newcastle University. Doctoral dissertation,.

Black, A., Peskett, L., MacDonald, A., Young, A., Spray, C., Ball, T., Thomas, H., Werritty, A., 2020. Natural flood management, lag time and catchment scale: results from an empirical nested catchment study. J. Flood Risk Manage. e12717 https://doi.org/10.1111/jfr3.12717.

Bouwes, N., Weber, N., Jordan, C.E., Saunders, W.C., Tattam, I.A., Volk, C., et al., 2016. Ecosystem experiment reveals benefits of natural and simulated beaver dams to a threatened population of steelhead (Oncorhynchus mykiss). Sci. Rep. 6, 28581. https://doi.org/10.1038/srep28581.

Burgess-Gamble, L., Ngai, R., Wilkinson, M., Nisbet, T., Pontee, N., Harvey, R., Kipling, K., Addy, S., Rose, S., Maslen, S., 2017. Working with natural processes – evidence directory. Environmental Agency Report No. SC150005.

Curran, J.H., Wohl, E.E., 2003. Large woody debris and flow resistance in step-pool channels, Cascade Range. Washington. Geomorphology 51 (1–3), 141–157.

Dadson, S.J., Hall, J.W., Murgatroyd, A., Acreman, M., Bates, P., Beven, K., Heathwaite, L., Holden, J., Holman, I.P., Lane, S.N., O'Connell, E., Penning-Rowsell, E., Reynard, N., Sear, D., Thorne, C., Wilby, R., 2017. A restatement of the natural science evidence concerning catchment-based 'natural' flood management in the UK. Proc. R. Soc. A Math. Phys. Eng. Sci. 473, 20160706. https://doi.org/10.1098/rspa.2016.0706.

Dixon, S.J., 2016. A dimensionless statistical analysis of logjam form and process. Ecohydrology 9, 1117–1129. https://doi.org/10.1002/eco.1710.

Dixon, S.J., Sear, D.A., 2014. The influence of geomorphology on large wood dynamics in a low gradient headwater stream. Water Resour. Res. 50 (12), 9194–9210.

Natural England, 1986. SSSI Citation, Wenlock Edge, Shropshire. Technical Report 1001712, available https://designatedsites.naturalengland.org.uk/PDFsForWeb/Citation/1001712.pdf.

Lidar Composite Digital Terrain Model England 2m resolution [ASC geospatial data], Scale 1:8000, Tiles: so5490, so5491, so5492, so5590, Updated: 5 January 2016, Open Government Licence, Using: EDINA LIDAR Digimap Service, <https://digimap.edina.ac.uk>, Downloaded: 2021-11-02 14:36:52.837.

Faulkner, D., Kjeldsen, T., Packman, J., Stewart, L., 2012. Estimating flood peaks and hydrographs for small catchments: Phase 1. SC090031. Environment Agency, Project.

Faustini, J.M., Jones, J.A., 2003. Influence of large woody debris on channel morphology and dynamics in steep, boulder-rich mountain streams, western Cascades. Oregon. Geomorphology 51 (1–3), 187–205. https://doi.org/10.1016/S0169-555X(02)00336-7.

Follett, E., Schalko, I., Nepf, H., 2020. Momentum and energy predict the backwater rise generated by a large wood jam. Geophysical Research Letters 47, e2020GL089346. https://doi.org/ 10.1029/2020GL089346.

Follett, E., Schalko, I., Nepf, H., 2021. Logjams with a lower gap: Backwater rise and flow redistribution beneath and through logjam predicted by two-box momentum balance. Geophysical Research Letters 48, e2021GL094279. https://doi. org/10.1029/2021GL094279.

Follett, E., Hankin, B., 2022. Investigation of effect of logjam series for varying channel and barrier physical properties using a sparse input data 1D network model. Environ. Model. Softw. 158, 105543 https://doi.org/10.1016/j.envsoft.2022.105543.

Follett, E., Wilson, C., (2020). Bedload sediment transport induced by channel-spanning instream structures. In River Flow,, 2020. Proceedings of the 10th Conference on Fluvial Hydraulics (Delft, Netherlands, 7–10 July 2020). CRC Press, London.

Garcia, M., Laursen, E.M., Michel, C., Buffington, J.M., 2000. The legend of A.F. Shields. J. Hydraul. Eng. 126 (9), 718–723. https://doi.org/10.1061/(asce)073309429(2000)126:9(718).

Geertsema, T.J., Torfs, P.J.J.F., Eekhout, J.P., Teuling, A.J., Hoitink, A.J., 2020. Wood-induced backwater effects in lowland streams. River Res. Appl. 36 (7), 1171–1182. https://doi.org/10.1002/rra.3611.

Gibling, M.R., Bashforth, A.R., Falcon-Lang, H.J., Allen, J.P., Fielding, C.R., 2010. Log jams and flood sediment buildup caused channel abandonment and avulsion in the Pennsylvanian of Atlantic Canada. J. Sediment. Res. 80 (3), 268–287.

Gonçalves, J.A., Moutinho, O.F., Rodrigues, A.C., 2016. Pole photogrammetry with an action camera for fast and accurate surface mapping. International Archives of the Photogrammetry, Remote Sensing and Spatial Information Sciences. 41, 571–575. https://doi.org/10.5194/isprsarchives-XLI-B1-571-2016.

Hankin, B., Metcalfe, P., Beven, K., Chappell, N.A., 2019. Integration of hillslope hydrology and 2D hydraulic modelling for natural flood management. Hydrol. Res. 50 (6), 1535–1548.

Hankin, B., Hewitt, I., Sander, G., Danieli, F., Formetta, G., Kamilova, A., Kretzschmar, A., Kiradjiev, K., Wong, C., Pegler, S., Lamb, R., 2020. A risk-based network analysis of distributed in-stream leaky barriers for flood risk management. Nat. Hazards Earth Syst. Sci. 20, 2567–2584. https://doi.org/10.5194/nhess-20-2567-2020.

Wallingford HydroSolutions, 2021. WINFAP 5 https://www.hydrosolutions.co.uk/software/winfap-5/.

Javernick, L., Brasington, J., Caruso, B., 2014. Modeling the topography of shallow braided rivers using Structure-from-Motion photogrammetry. Geomorphology 213, 166–182. https://doi.org/10.1016/j.geomorph.2014.01.006.

Julien, P., 2010. Erosion and sedimentation, 2nd ed. Cambridge University Press.

Keys, T.A., Govenor, H., Jones, C.N., Hession, W.C., Hester, E.T., Scott, D.T., 2018. Effects of large wood on floodplain connectivity in a headwater mid-Atlantic stream. Ecol. Eng. 118, 134–142.

Kjeldsen, T.R., 2007. Flood Estimation Handbook Supplementary Report No. 1 The revitalised FSR/FEH rainfall-runoff method. Centre for Ecology & Hydrology, Wallingford, UK.

Luhmann, T., Robson, S., Kyle, S., Boehm, J., 2019. Close-Range Photogrammetry and 3D Imaging, (3rd ed.). De Gruyter, p. 822p.

Metcalfe, P., Beven, K., Hankin, B., Lamb, R., 2017. A modelling framework for evaluation of the hydrological impacts of nature-based approaches to flood risk management, with application to in-channel interventions across a 29-km 2 scale catchment in the United Kingdom. Hydrol. Process. 31, 1734–1748. https://doi.org/10.1002/hyp.11140.

Muhawenimana, V., Wilson, C.A.M.E., Nefjodova, J., Cable, J., 2021. Flood attenuation hydraulics of channel-spanning leaky barriers. J. Hydrol. 596, 125731. https://doi.org/10.1016/j.jhydrol.2020.125731.

Nicholson, A.R., O'Donnell, G.M., Wilkinson, M.E., Quinn, P.F., 2020. The potential of runoff attenuation features as a Natural Flood Management approach. J. Flood Risk Manag. 13, 1–14. https://doi.org/10.1111/jfr3.12565.

Nisbet, T.R., Marrington, S., Thomas, H., Broadmeadow, S., Valatin, G., 2011. Slowing the flow at Pickering, Final Report to Defra, Project RMP5455.

Norbury, M., Phillips, H., Macdonald, N., Brown, D., Boothroyd, R., Wilson, C., Quinn, P., Shaw, D., 2021. Quantifying the hydrological implications of pre- and post-installation willowed engineered log jams in the Pennine Uplands. NW England. J. Hydrol. 603, 126855 https://doi.org/10.1016/j.jhydrol.2021.126855.

OTT (2021) Technical Data: OTT Orpheus Mini Water Level Logger. https://www.ott.com/products/water-level-1/ott-orpheus-mini-water-level-logger-3/productAction/outputAsPdf/.

Pinto, C., Ing, R., Browning, B., Delboni, V., Wilson, H., Martyn, D., Harvey, G.L., 2019. Hydromorphological, hydraulic and ecological effects of restored wood: findings and reflections from an academic partnership approach. Water Environ. J. 33, 353–365. https://doi.org/10.1111/wej.12457.

Ruiz-Villanueva, V., Piégay, H., Gurnell, A.M., Marston, R.A., Stoffel, M., 2016. Recent advances quantifying the large wood dynamics in river basins: new methods and remaining challenges. Rev. Geophys. 54, 611–652. https://doi.org/10.1002/2015RG000514.

Schalko, I., Lageder, C., Schmocker, L., Weitbrecht, V., Boes, R.M., 2019. Laboratory Flume experiments on the formation of spanwise large wood accumulations: Part II-effect on local scour. Water Resour. Res. 55, 4871–4885. https://doi.org/10.1029/2019WR024789.

Su, J., Bork, E., 2006. Influence of vegetation, slope, and lidar sampling angle on DEM accuracy. Photogramm. Eng. Remote Sens. 72 (11), 1265–1274.

Wenzel, R., Reinhardt-Imjela, C., Schulte, A., Bölscher, J., 2014. The potential of in-channel large woody debris in transforming discharge hydrographs in headwater areas (Ore Mountains, Southeastern Germany). Ecol. Eng. 71, 1–9. https://doi.org/10.1016/j.ecoleng.2014.07.004https://doi.org/10.1016/j.ecoser.2021.101330https://doi.org/10.1016/j.ecoser.2021.101330.

Westaway, R.M., Lane, S.N., Hicks, D.M., 2000. The development of an automated correction procedure for digital photogrammetry for the study of wide, shallow, gravel-bed rivers. Earth Surf. Proc. Land. 25, 209–226.

Wilcox, A.C., Wohl, E.E., 2006. Flow resistance dynamics in step-pool stream channels: 1. Large woody debris and controls on total resistance. Water Resour. Res. 42 (5).

Wohl, E., Beckman, N., 2014. Controls on the longitudinal distribution of channel-spanning logjams in the Colorado Front Range, USA. River Res. Appl. 30 (1), 112–131.

Wohl, E., Bledsoe, B.P., Fausch, K.D., Kramer, N., Bestgen, K.R., Gooseff, M.N., 2016. Management of large wood in streams: an overview and proposed framework for hazard evaluation. J Am Water Resour Assoc 52 (2), 315–335.

Wohl, E., Iskin, E., 2022. The transience of channel-spanning logjams in mountain streams. Water Resour. Res. 58, e2021WR031556 https://doi.org/10.1029/2021WR031556.

Woodget, A.S., Carbonneau, P.E., Visser, F., Maddock, I.P., 2015. Quantifying submerged fluvial topography using hyperspatial resolution UAS imagery and structure from motion photogrammetry. Earth Surf. Proc. Land. 40, 47–64. https://doi.org/10.1002/esp3613.